Twin-interface interactions in nanostructured Cu/Ag: Molecular dynamics study

Romuald Béjaud, Julien Durinck, Sandrine Brochard

Twin-interface interactions in nanostructured Cu/Ag: molecular dynamics study

R. Béjaud[a,1,*], J. Durinck[a], S. Brochard[a]

[a]*Institut Pprime, CNRS - Université de Poitiers - ENSMA, UPR 3346, Département de Physique et Mécanique des Matériaux, Bvd M. et P. Curie, SP2MI, BP 30179, 86962 Futuroscope Chasseneuil Cedex, France*

Abstract

The interaction of deformation twins with interfaces in nanostructured Cu/Ag is studied using molecular dynamics simulations. The influence of the interface structure on twin nucleation, propagation and thickening is analysed, and the role of the misfit interfacial dislocations mesh is detailed. In particular, we show that the interface can induce, directly or indirectly via Lomer dislocations, the nucleation of twinning dislocations. A thorough description of the involved mechanisms is given. Through this atomic scale approach, our study offers some useful understanding of the mechanical twinning process in nanolamellar composites, where twinning appears to be a common plasticity mechanism.

Keywords:
Deformation twins, Nanolayered materials, Heterophase interfaces, Molecular dynamics simulations

1. Introduction

When they are structured at the nanoscale, materials can exhibit properties different from those of the bulk. At this scale, the density of interfaces is very high, so that their role, which is already important in e.g. polycrystalline materials [1], becomes even more predominant over the bulk. In particular, interfaces govern mechanical properties in nanolayered or nanotwinned materials. Indeed, interfaces can interact in different ways with defects, acting as sources or barriers for dislocations, and leading to a modification of mechanical properties [2]. For example, it was shown that nanotwinned materials have improved strength, hardness and ductility [3, 4, 5, 6]. Several experimental and numerical studies demonstrated that in most cases twin boundaries (TBs) act as strong barriers for moving dislocations [7], explaining the increase of the strength in nanotwinned materials [8, 9, 10]. Similarly, interesting mechanical properties are encountered in nanolayered materials in which heterophase interfaces were found to be mainly responsible for a strengthening effect [11, 12].

Many of the bimetallic nanolayered composites are usually prepared using techniques like cold rolling, accumulative roll-bonding, and high-pressure torsion [13, 14]. A high amount of elastic strain is stored in materials during these severe plastic deformation (SPD) processes and is commonly released by mechanical twinning. It is well documented that the nucleation of partial dislocations and mechanical twinning is promoted at the nanoscale [15, 16]. This trend is especially true in metallic nanolayered materials. Indeed, recent experimental studies evidenced that twinning occurs at high stresses or strains in Cu/Nb and Cu/Ag bimaterials [17]. It is expected that heterophase interfaces play a crucial role on the onset of mechanical twinning. Depending on the interface type, twinning dislocations (TDs) may be nucleated from the interface directly in adjacent planes or transmitted from one layer to the other, or may be stopped at the interface leading to a strengthening effect [18].

Therefore the structure of heterophase interfaces is a key parameter for the plasticity mechanisms involved in these particular materials and a fundamental understanding of how interfaces interact with twins becomes essential. Because of the small length and time scales at which the elementary mechanisms occur, atomistic simulations appear to be relevant and efficient tools.

In this study, molecular dynamics simulations were performed to investigate, at the atomic scale, the interaction of twins with interfaces in a face centred cubic (FCC) bimetal, and more precisely the role of misfit dislocations on twin nucleation and thickening. Our strat-

*Corresponding author
[1]E-mail address: romuald.bejaud@univ-poitiers.fr (R. Béjaud).

egy was not to perfectly reproduce experimental situations such as those encountered during SPD processes, but rather to consider configurations for which twinning is promoted and twin/interface interactions easily analysed. The studied bimaterial is Cu/Ag, in which two different interfaces are commonly observed experimentally [17, 18, 19, 20] and shown to behave differently, especially regarding twin - interface interactions [17, 18]. Note that other FCC/FCC bimaterials may have similar interfacial features, in particular the Cu/Al system for which the lattice misfit is very close to that of the Cu/Ag system [21]. The chosen model is a self-supported thin film with one of the two interface types, referenced as "heterotwin" and "cube on cube" in the following . Twin/interface interactions were then studied according to the interface type. The simulation model is detailed in section 2.1 and a description of both interfaces is given in section 2.2. In section 3, we first analyse the role of the interface structure on mechanical twinning for a reference case, for a "cube on cube" interface (section 3.1) and for a "heterotwin" interface (section 3.2). Different sites for the first plasticity event are then considered in section 3.3, in order to assess the sensitivity of the simulation results to this parameter. Finally, in section 4, the role of misfit dislocations on twin nucleation and thickening is highlighted, with a focus on twin nucleation and thickening mechanisms implying misfit dislocations for a "heterotwin" interface in section 4.1, and for a "cube on cube" interface in section 4.2.

2. Model and methods

2.1. Simulation model

For this study a self-supported thin bimetallic film was built, as shown in figure 1, with the following dimensions: 18.4 nm × 29.2 nm × 16.7 nm along the $X = \langle 01\bar{1}\rangle$, $Y = \langle \bar{2}11\rangle$ and $Z = \langle 111\rangle$ directions (≈ 780,000 atoms). Periodic boundary conditions were applied in the X and Y directions and free surfaces were introduced in the Z direction. These particular crystallographic orientations have been considered in order to allow the introduction of the most common interfaces observed in the Ag-Cu multilayered materials and to promote Shockley dislocation nucleation and so twin nucleation. The chosen orientations also allow the introduction of specific surface defects, which can act as dislocation sources under mechanical stress. Steps are largely present at surfaces and a few studies showed their non-negligible role on dislocation nucleation [22, 23, 24]. Monoatomic surface steps have therefore been introduced in our systems along the $X = \langle 01\bar{1}\rangle$ dense direction. These surface steps can easily be created by removing one atomic layer over a portion of the Ag, Cu or both surfaces. However, because of the periodic boundary conditions, the steps have to be introduced in dipolar pairs.

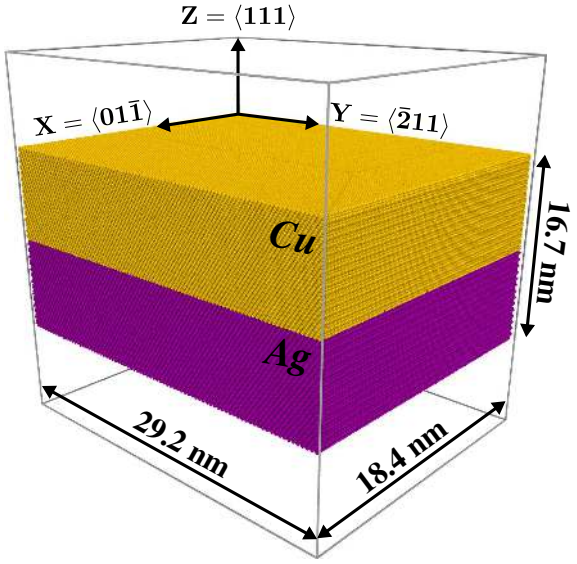

Figure 1: Thin bimetallic film containing two layers of the same size. Atoms are coloured according to their types (Ag in purple and Cu in yellow).

Molecular dynamics calculations were then performed using the LAMMPS code [25]. The embedded-atom method potential (EAM) of Williams et al. [26] was used to describe atomic interactions for Ag and Cu. For each of the two materials, this potential perfectly matches the lattice constants and closely reproduces the generalized stacking fault energies (GSFE) and the elasticity constants, which are key parameters when one is interested in plasticity and more particularly in twin formation. Moreover for bimetallic materials, this potential also allows interface sliding, which is quantified by the GSFE surface of the {111} Ag-Cu interface [27].

For each run after building the interface (described in section 2.2), a 300 K temperature was introduced by giving initial velocities to all atoms according to the Maxwell-Boltzmann distribution and the system was relaxed using an NPT integration according to the Nosé-Hoover thermostat, with zero pressure on each box faces. The system was subsequently compressed along the $Y = \langle \bar{2}11\rangle$ direction by deforming the simulation box at $\dot{\epsilon} = 10^8$ s^{-1} constant strain rate and using an NVT integration at 300 K, with a time step of 1 fs.

Different sets of atoms initial velocities for a given configuration were used to obtain reliable statistics from our simulations. Similar plasticity mechanisms were observed, showing a good reproducibility. A larger system with a different aspect ratio (33.4 nm × 41.8 nm × 20.0 nm, for nearly two million atoms) was also tested and similar results were obtained.

Post-processing was performed, using the Open Visualization Tool (OVITO) to visualise the atomic configurations [28]. The Dislocation Extraction Algorithm (DXA) was used to identify bulk and interface dislocations with their associated Burgers vector and an "home-made" algorithm based on local rotations was developed to identify twins. Note however that this algorithm, described in Appendix A, can only identify primary twins.

2.2. *Interface description*

Ag and Cu have a significantly different lattice parameter, respectively $a_{Ag} = 4.115$ Å and $a_{Cu} = 3.632$ Å at 300 K, for the interatomic potentials used, which implies a high lattice mismatch of $2\frac{a_{Ag}-a_{Cu}}{a_{Ag}+a_{Cu}} = 12.5\%$. The stress generated by this lattice mismatch can be relaxed by misfit dislocations at the interface. For Ag-Cu multilayered materials only two semicoherent interfaces structures are possible: the cube on cube (COC) close-packed orientation and the twin orientation (TO) [18, 19]. Both display a similar triangular mesh of misfit dislocations, as shown in Fig. 2.a.

To introduce the COC interface, we construct two slabs, one for each material. Ag and Cu layers are therefore aligned along the $Z = [111]$ direction while the other crystal orientations of both slabs are $X = [01\bar{1}]$ and $Y = [\bar{2}11]$. The TO interface is built by keeping the previous orientation for the Ag layer while the Cu slab is rotated by 180° around the Y axis, leading to the following orientations: $X = [0\bar{1}1]$, $Y = [\bar{2}11]$ and $Z = [\bar{1}\bar{1}\bar{1}]$. It can be noted that, since $8.a_{Ag} \approx 9.a_{Cu}$, the residual (coherency) strains are significantly reduced by choosing initial box lengths in the interface plane scaled to the average between $8.a_{Ag}$ and $9.a_{Cu}$. Thus, the box sizes are multiple of $\frac{\sqrt{2}}{2}\frac{(8.a_{Ag}+9.a_{Cu})}{2}$ along $X = \langle 01\bar{1}\rangle$ and $\frac{\sqrt{6}}{6}\frac{(8.a_{Ag}+9.a_{Cu})}{2}$ along $Y = \langle \bar{2}11\rangle$ [27].

Doing so, misfit dislocations are directly introduced at the interface, but without any core structure relaxation. The whole system (all atoms and box dimensions) is therefore relaxed by performing an energy minimization using the conjugate gradient method while keeping zero pressure on each box faces. Fig. 2.a shows the triangular mesh of intersecting dislocations obtained

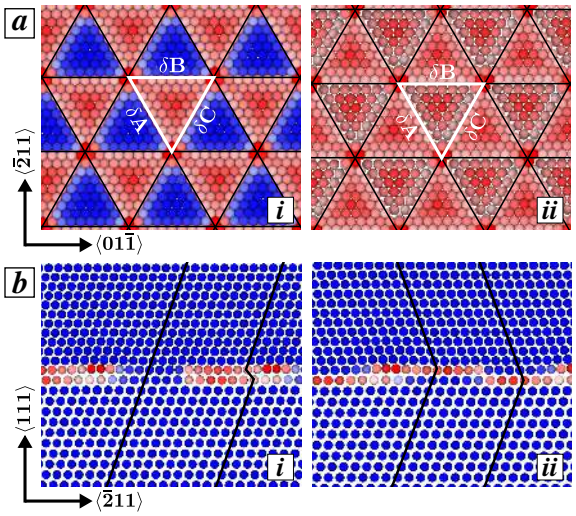

Figure 2: (a) Top view of Cu and Ag atoms along the interface (a.i) for a COC and (a.ii) for a TO interface. These views show the Shockley partial dislocations meshes (highlighted by the black lines), the associated triangular pattern (white segments), and the stacking faults distribution at the interface. (b) Side views along the $X = \langle 01\bar{1}\rangle$ direction show (b.i) coherent areas alternating with intrinsic stacking fault (ISF) areas in the case of a COC interface and (b.ii) twin faults areas successively in the Cu layer and in the Ag layer in the case of a TO interface. Atoms are coloured according to the centrosymmetry parameter (measure of the local deviation from centrosymmetry [29]). Atoms in blue are in a perfect FCC environment whereas atoms in red are in staking or twin faults.

then for both interface types. The three types of dislocations introduced are identified as Shockley partial dislocations, with Burgers vectors δA, δB and δC (according to the Thomson tetrahedron notation [30]) contained in the interface plane. These partial dislocations induce planar stacking faults at the interface. Depending on the interface type (COC or TO) the stacking faults are not similar and are differently distributed, as displayed in the side view of Fig. 2.b. The COC interface is composed of purely coherent areas alternating with intrinsic stacking fault (ISF) areas (Fig. 2.b.i.), whereas the TO interface is entirely composed of twin faults with the faulted areas successively in the Cu layer and in the Ag layer (Fig. 2.b.ii.).

3. Influence of the interface type on mechanical twinning

Bimetallic systems with each type of interface were submitted to uniaxial compression along the Y axis, as described in section 2.1. The tests detailed in section 3.1 and 3.2 were realised with two monoatomic steps on

the Ag surface, separated by 14.7 nm. Typical deformation sequences are displayed in Fig. 3, with corresponding curves in Fig. 4 and 5. Note however that because of thermal motion, some variance in the systems behaviours can be observed. In section 3.3, different nucleation sites are considered.

3.1. Cube on cube interface

For the system containing a COC interface, the onset of plasticity occurs for an average strain of 3.2%. This average, as well as all those given throughout section 3, is calculated over all simulations performed in the same configuration with different initial sets of velocities. As expected, the first plasticity event is the nucleation of a Shockley partial dislocation from one surface step. This dislocation then glides, leaving behind an intrinsic stacking fault, through the whole Ag layer and crosses the interface (Fig. 3.a.i). When this first dislocation reaches the Cu surface, two new Shockley partial dislocations are nucleated on both sides of the ISF, thus forming a small twin (Fig. 3.a.ii). This "rebound" or "reflection" mechanism for twinning was first pointed out by Christian who extended the mechanism described by Frank for perfect dislocations gliding on a same {111} plane [33] to Shockley partial dislocations in adjacent planes [34]. Then the twin extends via the nucleation from both surfaces of several Shockley dislocations in adjacent {111} planes along the TBs, again with the "rebound" mechanism. These onsets of plasticity and twinning correspond to the first stress drop in the light-blue stress-strain curve in Fig. 4.a. When the stress becomes too low, twinning stops spontaneously for an average applied strain of 3.6%; the corresponding snapshot is shown in Fig. 3.a.iii. In figure 4.b, the light-blue curve reports the proportion of atoms belonging to a twin, obtained with our own algorithm, versus applied strain. A first increase can be seen between 3.3% and 3.6% strain, consistent with the mechanisms observed in Fig. 3.a.i-iii.

The stress in the whole system increases anew until twinning starts again at 5.1% strain, with the nucleation of twinning dislocations from surfaces. Another stress drop can therefore be observed in the stress-strain curve (Fig. 4.a), and the proportion of "twinned" atoms increases a lot (Fig. 4.b). This ends at an applied strain of 5.4%, for which the stress starts rising up again, though more slightly than before the stress drops. In the same time, the proportion of "twinned" atoms increases slightly. This is explained by the activation of a different twinning mechanism, for which surfaces are not involved and Shockley partial dislocations are nucleated from the interface (Fig. 3.a.iv). This mechanism is described in detail in section 4.2. As evidenced in Fig. 4, it is "slower" than the "rebound" mechanism and it is not sufficient to completely relax the stress induced by the applied strain.

For the specific test shown in Fig. 3, the "interface" twinning mechanism is observed after two sequences of "surface" twinning mechanism, with two stress drops in the stress-strain curves. This global twinning sequence will be later noted SSI (for Surface Surface Interface). It is worth noting that for other tests (about half of the runs) the "interface" twinning mechanism is observed after only one "surface" twinning mechanism sequence; this is evidenced by only one stress drop in the stress-strain curve, and no plateau in the "twinned" atoms proportion curve. This twinning sequence is then denoted SI.

Finally at higher applied strain (above 7.0%), the stress is relaxed through the activation of other slip systems, with both Shockley partial and perfect dislocations (Fig. 3.a.v). These plasticity events are accompanied by a stress drop and a significant increase of the proportion of "twinned" atoms (Fig. 4).

3.2. Twin orientation interface

The simulation was then performed for a thin film containing the TO interface. The onset of plasticity is similar to that observed with a COC interface: nucleation of a Shockley partial dislocation from one surface step for a same average strain of 3.2% (see small stress drop in the red curve in Fig.4.a). This is easily explained by the fact that the nucleation mechanism is very localized at the surface so that the interface plays no role in it. The dislocation then glides through the Ag crystal leaving behind an ISF, but unlike for the COC interface it is stopped and stored at the interface (Fig. 5.a.i). However, in the absence of any other plasticity mechanism, the stress in the whole system increases again.

Plasticity starts again for an average strain of 5.5%, as shown in Fig. 5.a.ii with the nucleation from the Ag surface of a Shockley partial dislocation forming a twin with the first nucleated dislocation. Right after (or for some tests right before), a Lomer dislocation ($\frac{1}{2}\langle 110\rangle\{001\}$) in the Ag layer and a Shockley dislocation in the Cu layer are nucleated simultaneously from the interface (Fig. 5.a.ii). The mechanism through which the first Shockley partial dislocation interacts with the interface leading to the formation of a Lomer dislocation in Ag and a Shockley dislocation in Cu is explained in detail in section 4.1. Note that the Schmid factor is very high (0.47) for the Lomer dislocation, which promotes its gliding in the (100) plane. As the Lomer dislocation crosses the entire Ag crystal from

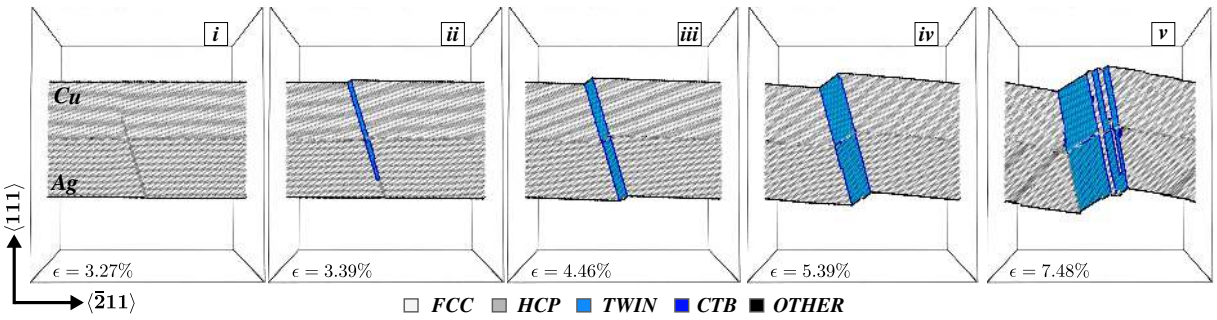

Figure 3: Plastic response of a thin Cu/Ag bimetallic film containing a COC interface under compression. (i-iii) Twin nucleation from a step on the Ag surface and (iv) twin thickening from the interface. (v) Subsequent plasticity mechanisms with twins and perfect dislocations nucleation. Atoms are shaded according to the common neighbour analysis (CNA) parameter (characteristic of the local crystal structure around an atom [31, 32]): atoms in black belong to a surface or a dislocation line, atoms in an ISF or a TB are in grey, and atoms in perfect FCC crystal arrangement are in light grey. Besides, atoms are coloured according to our own twin identification algorithm (Appendix A): in light blue for atoms belonging to a twin and in navy blue for atoms in a coherent twin boundary (CTB).

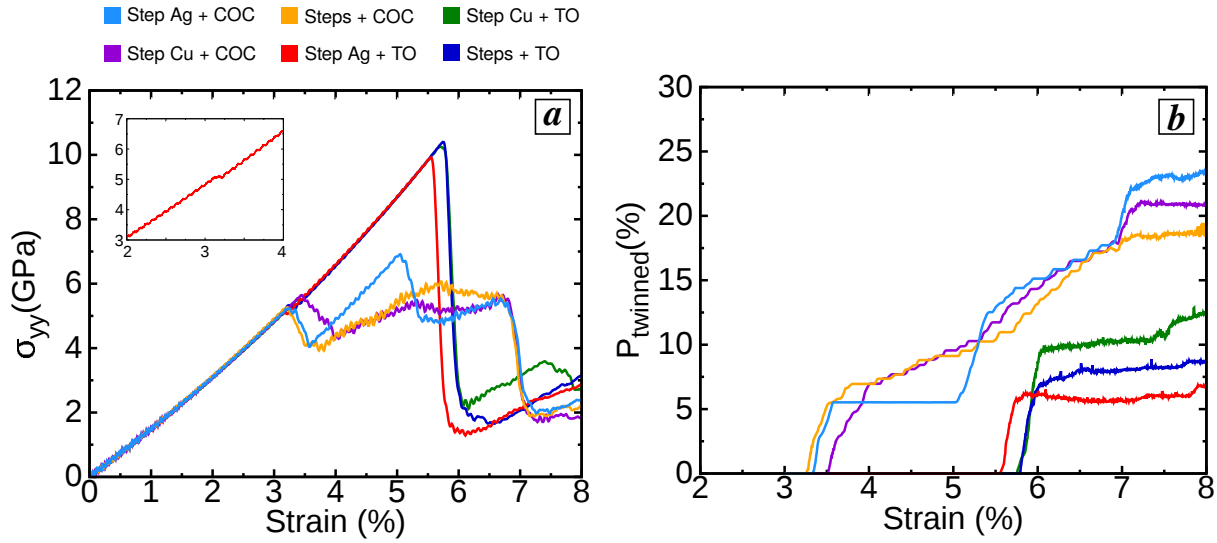

Figure 4: (a) Stress - strain curves and (b) total proportion of atoms belonging to a twin as a function of strain. Light blue, purple and yellow curves correspond to film configurations containing a COC interface and with respectively surface steps on the Ag, Cu and both surfaces. Red, green and navy blue curves correspond to film configurations containing a TO interface and with respectively surface steps on the Ag, Cu and both surfaces.

the interface to the surface, it causes the nucleation of several Shockley partial dislocations through successive occurrences of the mechanism illustrated in Fig 6. Indeed, when gliding the edge portion of the Lomer dislocation aligned along [01$\bar{1}$] can dissociate into a Frank dislocation and a Shockley dislocation (Fig. 6.b), according to [8]:

$$\begin{array}{ccccccc} \frac{1}{2}\left[0\bar{1}\bar{1}\right] & \rightarrow & \frac{1}{3}\left[1\bar{1}\bar{1}\right] & + & \frac{1}{6}\left[\bar{2}\bar{1}\bar{1}\right] \\ BD & \rightarrow & B\beta & + & \beta D \end{array} \quad (1)$$

using Thompson tetrahedron notation. The Shockley partial can glide easily in the ($\bar{1}$11) plane whereas the Frank partial dislocation is purely sessile. So the Shockley, Frank and Lomer dislocations are pinned at triple nodes that can only move along the [01$\bar{1}$] direction (Fig. 6.c). As the Shockley and Lomer dislocations bow out in their respective planes, the distance between the two triple nodes decreases and the Frank segment finally disappears according to the reaction reverse to reaction 1. Then the Shockley partial forms a loop, which extends in the whole crystal, and the Lomer dislocation is released (Fig. 6.d). While it continues to glide in its (100) plane, the Lomer dislocation can thus generate other Shockley partials in parallel ($\bar{1}$11) planes via the

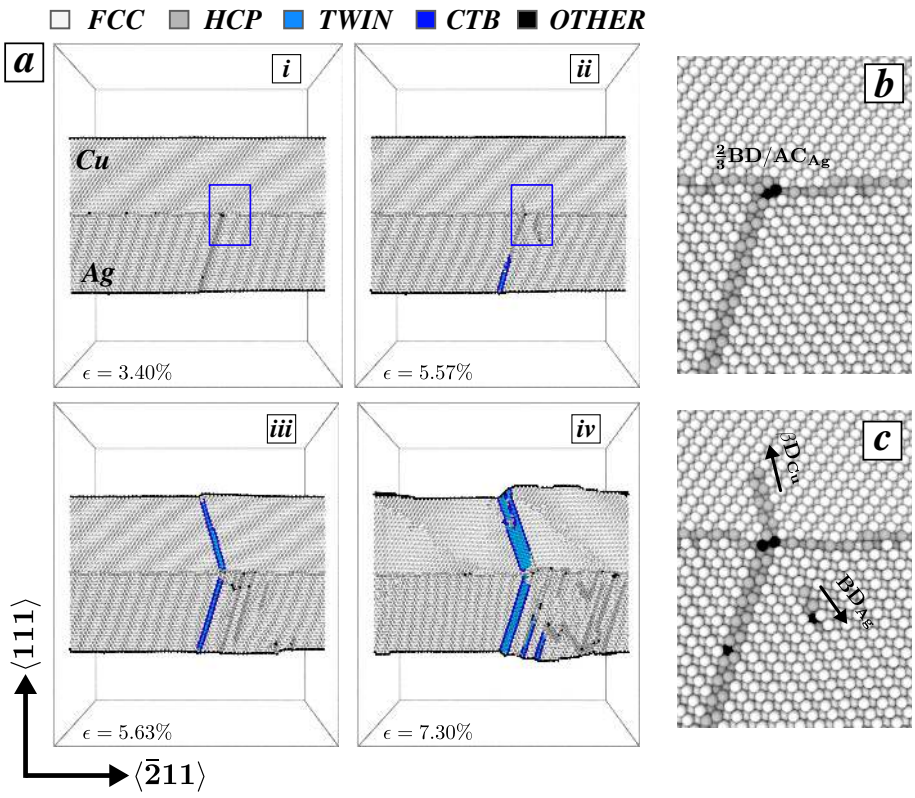

Figure 5: Plastic response of a thin Cu/Ag bimetallic film containing a TO interface under compression. (a.i-iii) Twin nucleation from a step on the Ag surface and Lomer dislocation nucleation from the interface. (a.iii-iv) Twin formation from the interface in the Cu layer. (b) Close-up view of the interface region framed in blue in (a.i), showing the interaction between a Shockley partial dislocation nucleated at the Ag surface and a misfit dislocation. (c) Close-up view of the interface region framed in blue in (a.ii), showing the formation of a Lomer dislocation in the Ag layer and a Shockley partial dislocation in the Cu layer. As in Fig. 3, atoms are coloured according to the CNA parameter and to our twin identification algorithm.

same mechanism, and can eventually lead to the formation of twins if these planes are adjacent (Fig. 5.a.iii-iv). We observe that this mechanism operates a few times as the Lomer dislocation crosses the Ag layer. Simultaneously, few Shockley dislocations are nucleated from the surface and along the first ISF in the Ag crystal, thus forming a twin (Fig. 5.a.ii-iv). In the Cu layer, the Shockley dislocation reaches the surface and induces the nucleation of new Shockley dislocations in {111} adjacent planes, thereby forming a twin (Fig. 5.b.iii-iv). All the formed twins are finally stopped at the interface.

These plasticity mechanisms all operate at the same time at 5.5% applied strain, resulting in an important stress drop which can be seen in the stress-strain curves (red curve in Fig. 4.a). There is also a significant increase of the "twinned" atom proportion because of the concomitant nucleation of twins in the Cu and Ag layers (red curve in Fig. 4.b), although the proportion of "twinned" atom is much less than for a COC interface at the same applied strain.

3.3. Varying nucleation sites

In order to test the influence of the first plasticity event location, steps were introduced on the Cu surface, along with or without steps on the Ag surface.

For all tested cases, Shockley dislocations are nucleated from steps. When steps are introduced on the Cu surface only, the yield point is slightly higher ($\approx$ 3.3%) than when steps are present on the Ag surface. This is consistent with higher intrinsic and unstable stacking fault energies in Cu. When steps are introduced on both surfaces, the first plasticity event therefore always starts at one of the Ag surface steps, and the yield point is similar to that described in sections 3.1 and 3.2 (yellow and navy-blue curves in Fig. 4.a).

For systems with a COC interface, the plastic response to the applied strain is similar whatever the first dislocation nucleation site. The two distinct twinning

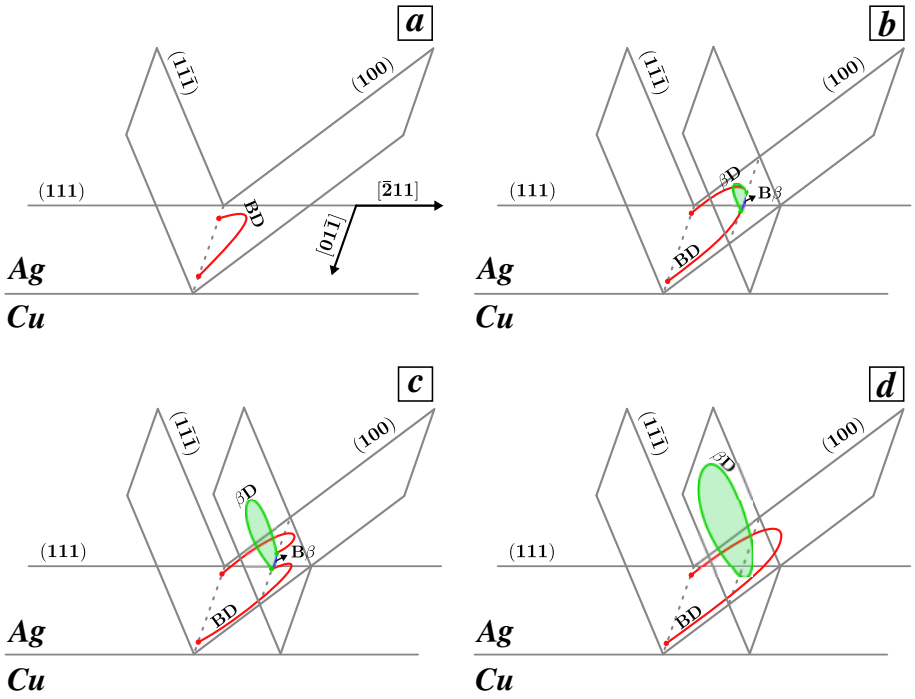

Figure 6: Schematic views of the mechanism leading to the formation of an isolated Shockley dislocation loop from a Lomer dislocation. (a) Starting configuration: Lomer dislocation (red line) gliding in a (100) plane. (b) Lomer dissociation (equation 1) into a Shockley partial dislocation in a (1$\bar{1}\bar{1}$) plane (green line) leaving behind an ISF (transparent green area) and a sessile Frank partial dislocation (blue line). (c) Extension of the Shockley and the Lomer dislocations, both being pinned by the sessile Frank dislocation. (d) Removal of the sessile Frank dislocation resulting in the formation of an isolated Shockley dislocation loop and release of the initial Lomer dislocation.

mechanisms (surface "rebound" and interface nucleation) are observed, but the twinning sequence can be different: SSI or SI (see section 3.1). It is worth noting that if steps are present on the Cu surface only, the "interface" twinning mechanism is always activated after only one "rebound" mechanism sequence (see purple curves in Fig. 4), according to a SI twinning sequence, which may be due to a higher yield strain. It should also be noted that when steps are introduced on both sides, the onset of plasticity in Ag is quickly followed by twin formation which relaxes a significant amount of stress (see yellow curve in Fig. 4.a), so that the steps on the Cu surface are in general not activated.

For systems containing a TO interface, the onset of plasticity is not strongly influenced by the location of the first nucleated dislocation: Shockley partial dislocations are always first nucleated from surface steps, glide through half part of the system and are stopped and stored at the interface. If surface steps are present on both sides of the system, this occurs almost simultaneously in both Cu and Ag parts; two Shockley dislocations are thus nucleated. As for the subsequent events, they depend significantly on the first nucleation sites: Lomer dislocations are formed only in the Ag crystal, when a Shockley partial in the Ag layer interacts with the interface. When steps are introduced on the Cu surface only, the first Shockley dislocation nucleates from the step in the Cu crystal. A new Shockley partial can later be nucleated from a random site on the Ag surface, for high enough accumulated stress. Then it glides and reaches the interface where its interaction with misfit dislocations gives rise to Lomer dislocation and another Shockley partial in Cu according to the mechanism mentioned in section 3.2.

4. Role of misfit dislocations

In section 3, it was evidenced that interfaces are not involved in the onset of plasticity (first dislocation nucleation), which occurs at surfaces. However, interactions between nucleated Shockley dislocations or TBs and interface misfit dislocations can lead to specific plasticity mechanisms. In particular, in section 4.1 we describe the Lomer dislocation nucleation mechanism observed for the TO interface (see section 3.2). Similarly, the twinning mechanism operating from the inter-

face and contributing to the twin extension in the case of a COC interface (see section 3.1) is detailed in section 4.2.

4.1. Nucleation of Lomer dislocation - TO interface

In the case of a TO interface, dislocation transmission is not possible due to a high angle disorientation between the two crystal layers. Dislocations nucleated from the surface of the film are therefore stopped and stored at the interface. These Shockley partial dislocations can then combine with misfit dislocations (Fig. 5.b), according to the following reaction:

$$\begin{array}{ccccc} \frac{1}{6}[211]_{Ag} & + & \frac{1}{6}\left[2\bar{1}\bar{1}\right]_{Ag} & \rightarrow & \frac{2}{3}[100]_{Ag}, \\ D\beta_{Ag} & + & B\delta_{Ag} & \rightarrow & \frac{2}{3}BD/AC_{Ag} \end{array} \quad (2)$$

When the accumulated stress is high enough, the newly formed dislocation dissociates according to the reaction:

$$\begin{array}{ccccccc} \frac{2}{3}[100]_{Ag} & \rightarrow & \frac{1}{2}\left[0\bar{1}\bar{1}\right]_{Ag} & + & \frac{1}{6}\left[\bar{2}\bar{1}\bar{1}\right]_{Cu} & + \\ & & \frac{1}{6}\left[2\bar{1}\bar{1}\right]_{Ag} & + & D_{res}, & \\ \frac{2}{3}BD/AC_{Ag} & \rightarrow & BD_{Ag} & + & \beta D_{Cu} & + \\ & & B\delta_{Ag} & + & D_{res} & \end{array} \quad (3)$$

where BD_{Ag} is a Lomer dislocation gliding in the Ag layer, βD_{Cu} is a Shockley partial dislocation gliding in the Cu layer, $B\delta_{Ag}$ is the initial recovered interfacial misfit dislocation and D_{res} is a residual interfacial dislocation (Fig. 5.c). The Shockley partial dislocation then crosses the entire Cu layer and induces the formation of a twin via the nucleation of successive Shockley dislocations from the free Cu surface. The interface thus directly plays the role of a source for twin nucleation.

Another mechanism of dislocation recombination which can lead to the formation of a Lomer dislocation has been observed for some runs, when two Shockley partial dislocations are nucleated successively in {111} adjacent planes in the Cu layer, thus forming an extrinsic stacking fault. These two Shockley dislocations collapse and form a super dislocation ($2\ D\beta_{Cu}$). The super dislocation rapidly dissociates into a sessile stair-rod dislocation ($\beta\delta_{Cu}$) stored at the interface and a Lomer dislocation BD_{Ag} which glides in a {100} plane in the Ag layer, according to the reaction:

$$\begin{array}{ccccc} \frac{1}{3}[211]_{Cu} & \rightarrow & \frac{1}{6}[011]_{Cu} & + & \frac{1}{2}\left[0\bar{1}\bar{1}\right]_{Ag}, \\ 2\ D\beta_{Cu} & \rightarrow & \beta\delta_{Cu} & + & BD_{Ag} \end{array} \quad (4)$$

In any case, for the TO interface, dislocation-interface interactions always lead to the nucleation of Lomer dislocations. Lomer dislocations were already observed experimentally [35, 36, 37, 38, 39], and in few simulations of deformed FCC metals it was found that they usually result from the interaction of a perfect dislocation and a TB [6, 8]. Lomer dislocations can dissociate and form Lomer-Cottrell locks [8, 30]. Such Lomer-Cottrell locks were also observed experimentally [36]. In our systems, the dissociation mechanism is not or only partially occurring, as seen in section 3.2. This is partly due to a high accumulated stress associated with a high Schmid factor which is sufficient to induce their easy gliding in {100} planes. Furthermore due to the proximity of surfaces, dislocations are rapidly eliminated which reduces their dissociation probability while gliding. As described in section 3.2, Lomer dislocations can often act as sources for Shockley dislocations and possibly deformation twins.

4.2. Twin dislocation nucleation induced by misfit dislocation - COC interface

Unlike the TO interface, the COC interface is fully permeable to dislocations; interface-dislocations interactions are therefore very limited. However, as seen in section 3.1, the interface can act as a source for TDs. This is always preceded by the formation of a twin via the dislocation "rebound" mechanism at the free surfaces. Therefore, due to this twin formation and the periodic boundary conditions, a rotation of the film around the $X = \langle 01\bar{1} \rangle$ axis happens (Fig. 7). The resolved shear stress in the interface plane (which was initially close to 0 GPa) then increases sufficiently to induce gliding of misfit dislocations. They therefore glide inside the interface until being stopped at the newly formed TB, where they interact with the latter. This interaction gives rise to the nucleation of a TD, as detailed hereafter. Similarly, the resolved shear stress along the interface inside the twin is not zero, so that misfit dislocations also glide inside the twinned part. They then interact with the second TB and contribute to the twin extension. Therefore, two mechanisms (one at each TB) lead to the extension of the newly nucleated twin.

The first one, displayed in Fig. 8, corresponds to the entry of the whole misfit dislocations pattern inside the twin, thus crossing one of the TBs. For the description, we choose to start with the initial configuration shown in Fig 8.a. This is actually not the real starting configuration, because when the twin is formed the position of the TB does not perfectly match with a specific component of the misfit dislocations pattern. The real configuration after the first ("rebound") twinning mechanism corresponds to that of Fig. 8.d, but we can assert that at some

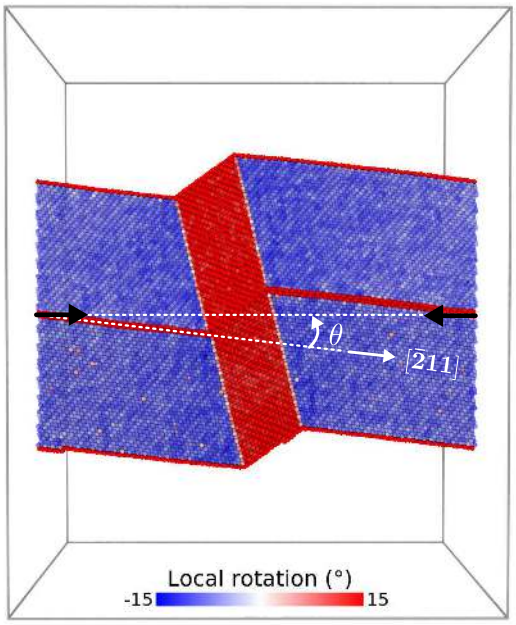

Figure 7: Thin Cu/Ag film containing a COC interface deformed plastically by twinning and rotated around the $X = \langle 01\bar{1} \rangle$ axis with an angle θ. Atoms are coloured according to the rotation of their local environment θ_i (compared to a non deformed initial configuration, see Appendix A). Black arrows correspond to the compression axis deformation and the white arrow to the $[\bar{2}11]$ direction belonging to the interface plane.

time during the process the configuration of Fig. 8.a will be reached without the emission of any TD.

Starting from the configuration displayed in Fig 8.a, the gliding of the misfit dislocations mesh across the TB is first accompanied by a reaction at node 1, producing as shown in Fig. 8.b a twinning Shockley dislocation gliding in the Cu layer along the TB ($D\beta$, blue line), an interface misfit dislocation inside the twin ($(\delta B)_T$, green line) and a residual interface dislocation stopped at the TB ($2/3B\beta$, yellow line). The two nodes 1 and 2 (Fig. 8.b), arising from the dissociation of node 1, move along the $[01\bar{1}]$ line direction of the two perfect lattice dislocations (BA and BC, red lines) locked at the intersection of the TB and the interface. While the TD $D\beta$ and the misfit dislocation $(\delta B)_T$ extend, node 1 (respectively 2) dissociates so as to form a new Shockley dislocation $(\delta A)_T$ (respectively $(\delta C)_T$) along the $[01\bar{1}]$ direction between nodes 1 and 3 (respectively between nodes 2 and 4), as shown in Fig. 8.c. The three Shockley dislocations $(\delta B)_T$, $(\delta A)_T$ and $(\delta C)_T$ between nodes 1-2, 1-3 and 2-4 respectively make up the sketch of the "triangular" ISF pattern inside the twin. As node 1 (respectively 2) moves along the $[01\bar{1}]$ direction, the perfect dislocation BA (respectively BC) progressively disappears until node 1 reaches node 5 (respectively node 2 reaches node 6). At this point, because of the periodicity of the interface pattern along the $[01\bar{1}]$ direction, node 5 is equivalent to node 2 (respectively node 6 is equivalent to node 1), so that nodes 1 and 2 recombine. The interface dislocation $(\delta B)_T$ between nodes 1 and 2 can thus glide freely along the interface inside the twin, and the twinning Shockley dislocation $D\beta$ can glide freely along the TB. The whole faulted "triangular" pattern then crosses the TB with misfit dislocations δC and δA transmitted through nodes 3 and 4, as indicated in Fig. 8.d. This leaves behind the residual dislocation $2/3B\beta$ locked at the TB. Once the misfit Shockley partial dislocations δC and δA have gone through the TB, the last partial dislocation δB (closing the ISF in the perfect crystal) reacts at nodes 3 and 4 with this residual dislocation, so as to form the perfect lattice dislocations BC and BA at the TB and allow the extension of misfit dislocations $(\delta A)_T$ and $(\delta C)_T$ inside the twin (Fig. 8.e). Nodes 3 and 4 finally recombine, thereby closing the triangular ISF pattern in the twinned crystal part. At the end of this process, the misfit dislocations pattern has entirely crossed the TB, the two perfect lattice dislocations BC and BA have been formed and connected at one node, and the whole system is therefore back into the initial configuration of Fig. 8.a. However, during this process a TD has been emitted in the Cu layer, thus contributing to the twin extension.

The second mechanism, displayed in Fig. 9, corresponds to the exit from the twin of the whole misfit dislocations pattern. Fig. 9.a shows the starting configuration for the description. As previously, this configuration, though not being the real starting one, will necessarily be reached during the process. From this configuration, the first step is a reaction at node 1 (Fig. 9.a), producing the TD βD (blue line in Fig. 9.b) in the Ag layer and the misfit dislocation δB along the $[01\bar{1}]$ direction between nodes 1 and 2 (Fig. 9.b), arising from the dissociation of the initial node 1. As the TD βD extends, nodes 1 and 2 move along the $[01\bar{1}]$ direction, until node 1 (respectively node 2) recombines with node 2' (respectively node 1'), the periodic image of node 2. The misfit dislocation $(\delta B)_T$ is then completely transmitted through the TB and the TD βD can glide freely (Fig. 9.c). The final step corresponds to the complete crossing of the TB by misfit dislocations $(\delta A)_T$ and $(\delta C)_T$ through node 1, which dissociates into nodes 1 and 3 as indicated in Fig. 9.d. This is accompanied by the formation of a residual dislocation $2/3B\beta$, locked along the $[01\bar{1}]$ direction, between nodes 1 and 3. Once the two misfit dislocations $(\delta A)_T$ and $(\delta C)_T$ have been

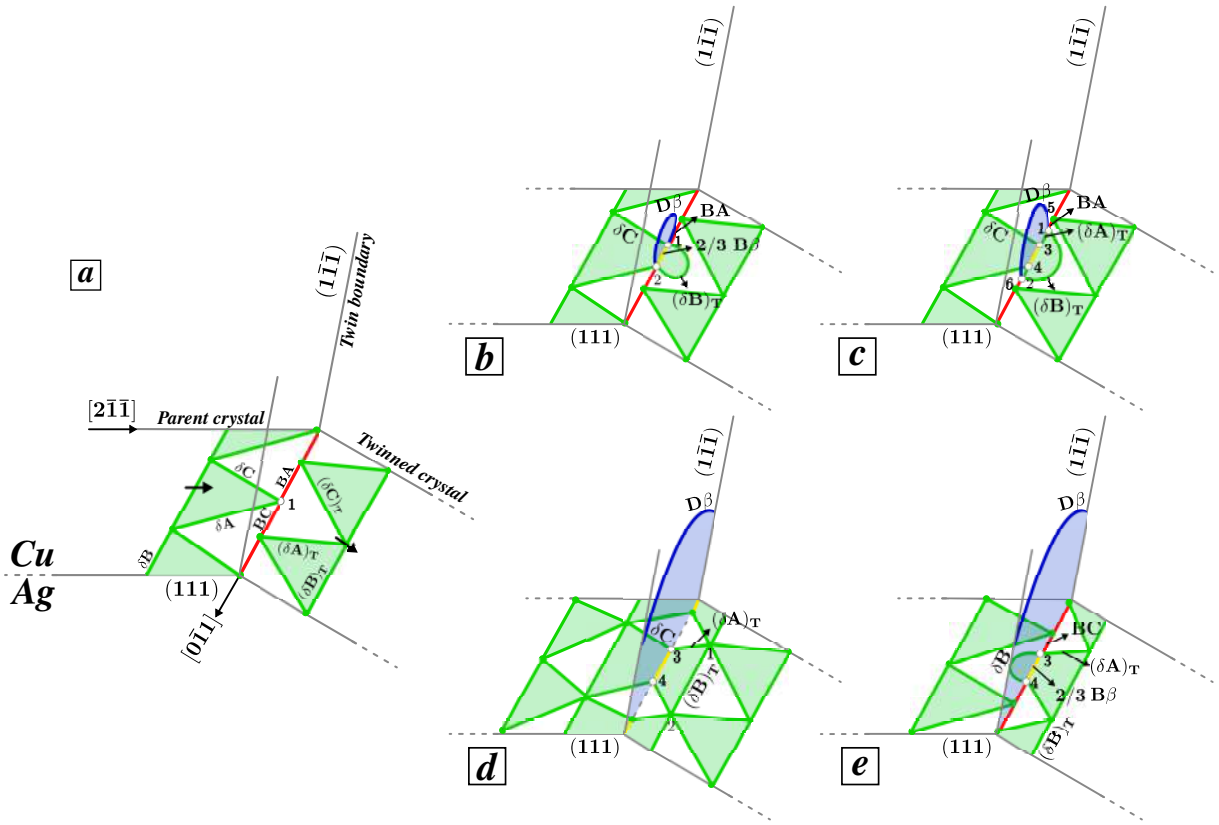

Figure 8: Schematic views of the entry of the misfit dislocations pattern inside the twin, leading to the nucleation of a twinning dislocation in the Cu layer (see text for details). The green lines represent Shockley partial dislocations gliding along the interface with their associated ISF (green areas). The blue line corresponds to a Shockley dislocation gliding along the twin boundary with its associated ISF (blue area). The red line is associated to perfect lattice dislocations and the yellow line to a residual dislocation locked at the intersection of the interface and the twin boundary. The black arrows in (a) indicate the direction of the misfit dislocations motion.

transmitted, the triangular ISF pattern has crossed the TB and the system is back into the initial configuration of Fig. 9.a. Nevertheless, a TD has been emitted in the Ag layer, increasing the twin size.

5. Discussion

Four main mechanical twinning processes are observed in our simulations:

- twin nucleation at surfaces;
- twin nucleation in copper and twin nucleation and extension in silver from Lomer dislocations (systems with a TO interface);
- twin extension via Shockley dislocation "rebound" at surfaces;
- twin extension from the COC interface.

For all runs, the first Shockley partial dislocation is nucleated at surface steps, purposefully introduced. Hence, twins are nucleated from surfaces in most cases. We also observe twin nucleation directly from the TO interface, and indirectly after the formation of a Lomer dislocation. Such dislocations are often encountered experimentally, especially under extreme loading conditions, close to those considered in MD simulations. In our simulations, their nucleation stems from the absence of permeability of the TO interface to dislocations, which induces specific reactions between the first nucleated dislocation and interfacial dislocations. The Lomer dislocation dissociation can then lead to the formation of twins. Conversely, twin nucleation from the COC interface is not seen in our systems, most likely because surface steps are most efficient sources for the first TD in these systems. In their study of Cu/Ag nanolayers subjected to out of plane tension, Li and Chew [27] underscore twin nucleation directly from a COC inter-

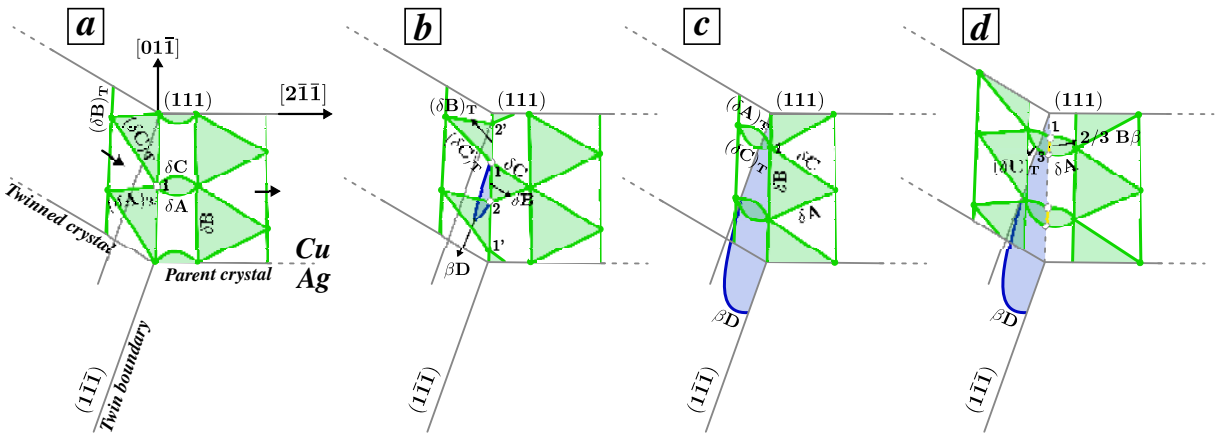

Figure 9: Schematic views of the exit of the misfit dislocations pattern from the twin, leading to the nucleation of a TD in the Ag layer (see text for details). The lines colour coding is the same as that of Fig. 8. The black arrows in (a) indicate the direction of the misfit dislocations motion.

face. It ensues there from a planar-to-wavy interlayer transition and the subsequent development of high stress concentrations at interfaces. Twin nucleation from the Cu/Ag interface of nanolamellar composites is also suggested in an experimental study [18]. In such systems, intrinsic interfacial defects such as atomic steps are deemed to be TD sources.

The "rebound" mechanism initially proposed by Frank [33] is at the origin of the first twin extension for systems with a COC interface. It is much less important for systems with a TO interface, because of its absence of permeability to dislocations, so that the "rebound" can not operate from the Cu surface to the Ag surface and vice versa. However, it can sligthly participate to twin extension in these systems, through one "rebound" at one of the surface of a Shockley dislocation nucleated from the interface (directly or indirectly after a Lomer dislocation dissociation). Similar "rebound" or "reflection" mechanisms at surfaces have been observed in previous numerical studies [40, 41]. "Rebounds" at interfaces or grain boundaries have also been postulated, seen in MD simulations and suggested in expertimental studies [42, 43, 44]. If the reflecting dislocation is a partial dislocation, the mechanism produces twins [34, 40, 41, 44], as observed in our study. Anyway, the incipient dislocation velocity is of prime importance and should be close to the sound speed for the surface "rebound" to occur [33, 41]. Such high velocities are commonly attained in MD simulations, and expected experimentally under the extreme loading conditions frequently encountered at the nanoscale.

Finally, a crucial process revealed by our simulations is the twin extension from the COC interface. It is a consequence of the tilt of the interface plane with respect to the compression axis, which entails the movement of interfacial dislocations. Though the loading directions might not be the same, this twin thickening mechanism may be at work during SPD processes. In particular if the loading axis is normal to the interface, the Schmid factor on misfit dislocations, which is initially zero, will change to non zero if a slight tilt of the interface arises. Such a tilt is expected, at least locally, as soon as a twin has been formed and it can be noticed in experiments [18]. This twin thickening mechanism from the COC interface may well be also involved in the twin extension observed in Li and Chew simulations [27].

The twin extension from the COC interface and the twin nucleation/extension ensuing from Lomer dissociation for systems with a TO interface are not depending upon the presence of free surfaces, by contrast to the surface "rebound" mechanism, which besides needs high speed dislocations. They are thus particularly relevant to nanolayered systems. For these mechanisms, the structure of the interface and the misfit interfacial dislocations mesh are determining. Also, because of the absence of permeability of the TO interface to TDs, the twin extension is limited, and the formed twins are smaller but may be more numerous than for the COC interface, for which the proportion of "twinned" atoms is higher.

6. Conclusion

Our results highlight how heterophase interface structure impacts the different steps of the mechanical twinning processes (nucleation, propagation and

thickening) and therefore the size of the formed twins in nanostructured Cu/Ag. Designing multilayered materials in order to tune their mechanical properties is still a hot topic and manipulating the deformation mechanisms as twinning will allow to combine mechanical properties of nanolayered and nanotwinned materials. In this respect, this study provides useful keys for the understanding of twin-interface interaction mechanisms and supports the idea that twinning is facilitated by heterophase interfaces.

Acknowledgements

This work pertains to the French Government program "Investissements d'Avenir" (LABEX INTERACTIFS, reference ANR-11-LABX-0017-01). Computations have been performed on the supercomputer facilities of the Mésocentre de calcul Poitou-Charentes and also using HPC resources from GENCI - CINES/IDRIS (Grant 2016 - [x2016097588]).

Appendix A. Twin identification algorithm

For this study, a code has been developed to identify and follow over the time the number of "twinned" atoms, in each twin or in the whole system. This algorithm involves a post processing of output atomic positions files, once the run is done.

The identification of twins is based on two key quantities, calculated for each atom i:

- the local rotation associated with plasticity θ_i^{plast}; its calculation is detailed below;
- the CNA parameter f_i^{CNA}, which can be obtained directly from LAMMPS.

Indeed, to belong to a twin, an atom must fulfill both conditions:

- the local rotation associated with plasticity θ_i^{plast} must be close to the theoretical value 19.47° involved by twin formation;
- the CNA parameter must be that of a perfect FCC structure, $f_i^{CNA} = 1$, since an atom inside a twin is in a perfect FCC environment.

To work properly, the code needs a reference file system corresponding to the initial state. This reference system is defined by the user; it should preferably be not deformed and must not contain dislocation. The first step of the algorithm consists in searching the nearest neighbours (inside a given cut-off radius set by the user) of each atom of the reference file system, and memorising their identification number (ID, as assigned e.g. by LAMMPS) into a table. This table will be useful at different stages, especially for the transformation matrix calculation and for searching twins.

Calculation of local rotation. To calculate the local rotation for each atom i, we first need to determine the deformation gradient tensor $\mathbf{F}^i$ needed to pass from one reference system to the distorted system to be considered, such that

$$\mathbf{D}^{ij} = \mathbf{F}^i.\mathbf{d}^{ij}$$

where $\mathbf{d}^{ij}$ and $\mathbf{D}^{ij}$ are the vectors going from the atom i to one of its neighbour j in the reference and the distorted configurations, respectively. The tensor $\mathbf{F}^i$ that best maps the neighbouring environment of the atom i is determined by linear regression over the first nearest neighbours of i. The deformation gradient tensor $\mathbf{F}^i$ in then decomposed into two tensors by a polar decomposition:

$$\mathbf{F}^i = \mathbf{R}^i.\mathbf{U}^i$$

with $\mathbf{R}^i$ being the orthogonal rotation tensor and $\mathbf{U}^i$ the symmetric right stretch tensor.

The rotation matrix can then be written as a function of the rotation angle θ_i about the rotation axis, defined by the unit vector $\overrightarrow{u}(u_x,u_y,u_z)$:

$$\mathbf{R}^i = \begin{pmatrix} u_x^2(1-c)+c & u_xu_y(1-c)-u_zs & u_xu_z(1-c)+u_ys \\ u_xu_y(1-c)+u_zs & u_y^2(1-c)+c & u_yu_z(1-c)-u_xs \\ u_xu_z(1-c)-u_ys & u_yu_z(1-c)+u_xs & u_z^2(1-c)+c \end{pmatrix}$$

with $s = \sin(\theta_i)$ and $c = \cos(\theta_i)$.

The local rotation θ_i associated to an atom i is next calculated from the trace of $\mathbf{R}^i$:

$$\cos(\theta_i) = \frac{1}{2}\left[tr\left(\mathbf{R}^i\right) - 1\right]$$

To determine the sign of θ_i, the orientation of the rotation axis $\overrightarrow{u}(u_x,u_y,u_z)$ and $\sin(\theta_i)$ are also extracted from the rotation matrix $\mathbf{R}^i$. However, this calculated rotation extracted from the rotation matrix comprises not only the local rotation due to plasticity (θ_i^{plast}) but also a global rotation (θ_o) of the whole system which is induced in our case by the presence of periodic boundary conditions. The local rotation θ_i can therefore be expressed as follows:

$$\theta_i = \theta_o + \theta_i^{plast} \tag{A.1}$$

θ_o can be calculated by averaging θ_i over all atoms that have not been plastically deformed, for which $\theta_i^{plast} = 0$.

These atoms are identified through a regular monitoring of the CNA parameter: it should remain zero for atoms that have not been plastically deformed. Once θ_o is determined, θ_i^{plast} is obtained from equation (A.1).

Twin search algorithm. When the local plastic rotation is known, the twin search can begin. We first create a function f^{twin} which will return, for an atom i, the twin ID to which it belongs. If the atom does not belong to a twin, the result will be zero ($f_i^{twin} = 0$). For twin search, the atoms of the system are first scanned randomly until one is found respecting both conditions described above ($\theta_i^{plast} \approx 19.47°$ and $f_i^{CNA} = 1$). The atom i is then considered as belonging to a new twin, to which an ID is assigned, and f_i^{twin} is set to this ID. The next operation consists in searching all the other atoms in that same twin. To do this, starting from the atom i we look step by step if neighbour atoms are in the twin configuration (see Fig. A.1). If some neighbour atoms fulfil the twin conditions, they are assigned the corresponding twin ID and they are memorized to be later analysed. This operation is repeated until all the atoms belonging to the twin are identified. We can therefore randomly search for another atom corresponding to a twin type configuration and make a new step by step search. When all the atoms of the system have been analysed, all twins have been found and the ID of the last identified twin corresponds to the number of twins in the whole system.

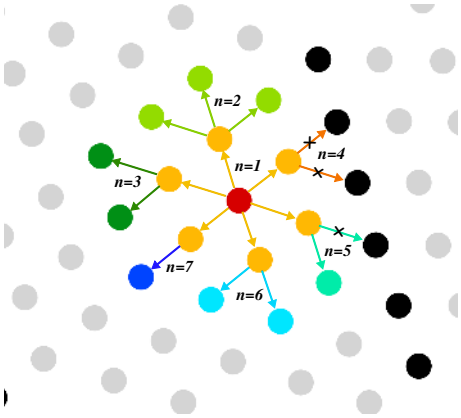

Figure A.1: Seven first iterations of the step by step twin identification algorithm; in light grey the atoms corresponding to a perfect FCC crystal structure (CNA = 1) and in black the atoms belonging to a stacking fault (CNA = 2). Colours are superimposed to display the growth of the detected twinned zone.

Identification of twin boundaries. Atoms in a coherent twin boundary (CTB) are characterized by a CNA parameter equal to 2, corresponding to a compact hexagonal local structure. Thus they have not been identified in the previous step of the algorithm. Here again, a function (f^{tb}) is created, which will return, for an atom i belonging to a CTB, the ID of the twin considered. For example, if an atom i is in the boundary of the twin whose ID is 2 then $f_i^{tb} = 2$. On the other hand, if the atom is not in a CTB, the returned value will be zero ($f_i^{tb} = 0$). Here only atoms whose CNA parameter is equal to 2 are scanned. These atoms can belong either to a stacking fault (ISF), generated by one Shockley dislocation, or to a CTB. To differentiate between ISF and CTB, it is sufficient to look if a twin has been identified in the close proximity of the scanned atom; if it is the case, the ID of the nearby twin will be assigned to it ($f_i^{tb} = ID$). Thus, an atom whose CNA parameter is 2 is considered in a CTB if it has at least two neighbour atoms j belonging to a twin ($f_j^{twin} = ID$) and two others belonging to a non-twinned crystal ($f_j^{twin} = 0$).

Final check. In some cases, a group of atoms may be erroneously identified as a twin by the algorithm. It is the case for example for atoms crossed by a full lattice dislocation: the local rotation induced by this dislocation is close to 19.47° and after the passage of the dislocation these atoms are again in a perfect FCC environment. Therefore, this group of atoms has been identified as a twin by the algorithm but cannot be considered as a "real" twin and must be removed from the list. Such a group of atoms has no CTB associated to it, so that the final check is to test if the twins identified by the algorithm have a CTB associated with them, in which only case they are kept in the twin list.

References

[1] A. Sutton, R. Balluffi, Interfaces in Crystalline Materials, Oxford University Press, 1995.
[2] I. Beyerlein, M. Demkowicz, A. Misra, B. Uberuaga, Defect-interface interactions, Progress in Materials Science 74 (2015) 125–210.
[3] L. Lu, Y. Shen, X. Chen, L. Qian, K. Lu, Ultrahigh strength and high electrical conductivity in copper, Science 304 (2004) 422–6.
[4] L. Lu, X. Chen, X. Huang, K. Lu, Revealing the maximum strength in nanotwinned copper, Science 323 (2009) 607–10.
[5] A. Stukowski, K. Albe, D. Farkas, Nanotwinned fcc metals: Strengthening versus softening mechanisms, Phys. Rev. B 82 (2010) 224103.
[6] K. A. Afanasyev, F. Sansoz, Strengthening in gold nanopillars with nanoscale twins, Nano Letters 7 (2007) 2056–62.
[7] L. Priester, J.-P. Couzinié, B. Décamps, S. Lartigue-Korinek, Interactions between dislocations and interfaces – consequences for metal and ceramic plasticity, International Journal of Materials Research 101 (2010) 1202–10.
[8] Z. Wu, Y. Zhang, D. Srolovitz, Dislocation twin interaction mechanisms for ultrahigh strength and ductility in nanotwinned metals, Acta Materialia 57 (2009) 4508–18.

[9] C. Deng, F. Sansoz, Enabling ultrahigh plastic flow and work hardening in twinned gold nanowires, Nano Letters 9 (2009) 1517–22.

[10] Y. Cao, Y. Wang, X. An, X. Liao, M. Kawasaki, S. Ringer, T. Langdon, Y. Zhu, Grain boundary formation by remnant dislocations from the de-twinning of thin nano-twins, Scripta Materialia 100 (2015) 98–101.

[11] A. Misra, H. Krug, Deformation behavior of nanostructured metallic multilayers, Advanced Engineering Materials 3 (2001) 217–22.

[12] A. Misra, J. Hirth, R. Hoagland, Length-scale-dependent deformation mechanisms in incoherent metallic multilayered composites, Acta Materialia 53 (2005) 4817–24.

[13] Y. Tian, Z. Zhang, Stability of interfaces in a multilayered Ag-Cu composite during cold rolling, Scripta Materialia 68 (2013) 542–5.

[14] W. Han, J. Carpenter, J. Wang, I. Beyerlein, N. Mara, Atomic-level study of twin nucleation from face-centered-cubic/body-centered-cubic interfaces in nanolamellar composites, Applied Physics Letters 100 (2012) 011911.

[15] M. Chen, E. Ma, K. J. Hemker, H. Sheng, Y. Wang, X. Cheng, Deformation twinning in nanocrystalline aluminum, Science (2003) 1275–7.

[16] G. Dehm, S. Oh, P. Gruber, M. Legros, F. Fischer, Strain compensation by twinning in Au thin films: Experiment and model, Acta Materialia 55 (2007) 6659–65.

[17] S. Zheng, J. Wang, J. Carpenter, W. Mook, P. Dickerson, N. Mara, I. Beyerlein, Plastic instability mechanisms in bimetallic nanolayered composites, Acta Materialia 79 (2014) 282–91.

[18] X. H. An, S. M. Zhu, Y. Cao, M. Kawasaki, X. Z. Liao, S. P. Ringer, J. F. Nie, T. G. Langdon, Y. T. Zhu, Atomic-scale investigation of interface-facilitated deformation twinning in severely deformed Ag-Cu nanolamellar composites, Applied Physics Letters 107 (2015).

[19] J. Wang, I. J. Beyerlein, N. A. Mara, D. Bhattacharyya, Interface-facilitated deformation twinning in copper within submicron Ag-Cu multilayered composites, Scripta Materialia 64 (2011) 1083–6.

[20] Y. Tian, Z. Zhang, Bulk eutectic Cu-Ag alloys with abundant twin boundaries, Scripta Materialia 66 (2012) 65 –8.

[21] R. Li, H. B. Chew, Closed and open-ended stacking fault tetrahedra formation along the interfaces of Cu-Al nanolayered metals, Philosophical Magazine 95 (2015) 2747–63.

[22] S. Brochard, P. Beauchamp, J. Grilhé, Dislocation nucleation from surface steps: Atomistic simulation in aluminium, Philosophical Magazine A 80 (2000) 503–24.

[23] P. Hirel, S. Brochard, L. Pizzagalli, P. Beauchamp, Effects of temperature and surface step on the incipient plasticity in strained aluminium studied by atomistic simulations, Scripta Materialia 57 (2007) 1141–4.

[24] V. Navarro, O. R. de la Fuente, A. Mascaraque, J. M. Rojo, Uncommon dislocation processes at the incipient plasticity of stepped gold surfaces, Phys. Rev. Lett. 100 (2008) 105504.

[25] S. Plimpton, Fast parallel algorithms for short-range molecular dynamics, Journal of computational physics 117 (1995) 1–19.

[26] P. Williams, Y. Mishin, J. Hamilton, An embedded-atom potential for the Cu-Ag system, Modelling and Simulation in Materials Science and Engineering 14 (2006) 817.

[27] R. Li, H. B. Chew, Planar-to-wavy transition of Cu-Ag nanolayered metals: a precursor mechanism to twinning, Philosophical Magazine 95 (2015) 1029–48.

[28] A. Stukowski, Visualization and analysis of atomistic simulation data with OVITO the open visualization tool, Modelling and Simulation in Materials Science and Engineering 18 (2010) 015012.

[29] C. L. Kelchner, S. J. Plimpton, J. C. Hamilton, Dislocation nucleation and defect structure during surface indentation, Phys. Rev. B 58 (1998) 11085–8.

[30] J. P. Hirth, J. Lothe, Theory of Dislocations, 1982.

[31] J. D. Honeycutt, H. C. Andersen, Molecular dynamics study of melting and freezing of small Lennard-Jones clusters, The Journal of Physical Chemistry 91 (1987) 4950–63.

[32] D. Faken, H. Jónsson, Systematic analysis of local atomic structure combined with 3D computer graphics, Computational Materials Science 2 (1994) 279–86.

[33] F. C. Frank, On slip bands as a consequence of the dynamic behaviour of dislocations, in: Report of a conference on strength of solids, University of Bristol, 1948, pp. 46–51.

[34] J. W. Christian, A theory of the transformation in pure cobalt, Proceedings of the Royal Society of London A: Mathematical, Physical and Engineering Sciences 206 (1951) 51–64.

[35] A. Korner, H. P. Karnthaler, The study of glide dislocation loops on {001} planes in a f.c.c. alloy, Philosophical Magazine A 42 (1980) 753–62.

[36] A. Korner, H. P. Karnthaler, Weak-beam studies of composite dislocations and dislocations gliding on (001) planes in silver, Philosophical Magazine A 44 (1981) 275–84.

[37] J. Bonneville, J. Douin, On the asymmetrical dissociation of Lomer dislocations, Philosophical Magazine Letters 62 (1990) 247 –51.

[38] M. J. Mills, P. Stadelmann, A study of the structure of Lomer and 60° dislocations in aluminium using high-resolution transmission electron microscopy, Philosophical Magazine A 60 (1989) 355–84.

[39] O. Hardouin Duparc, J.-P. Couzinié, J. Thibault-Pénisson, S. Lartigue-Korinek, B. Décamps, L. Priester, Atomic structures of symmetrical and asymmetrical facets in a near $\Sigma = 9\{221\}$ tilt grain boundary in copper, Acta Materialia 55 (2007) 1791–800.

[40] P. Hirel, Étude par simulations à l'échelle atomique de la formation de boucles de dislocation à partir d'irrégularités de surface d'un métal contraint, Phd thesis, University of Poitiers, 2008.

[41] Q.-J. Li, J. Li, Z.-W. Shan, E. Ma, Strongly correlated breeding of high-speed dislocations, Acta Materialia 119 (2016) 229–41.

[42] S. A. Dregia, J. P. Hirth, A rebound mechanism for Lomer dislocation formation in strained layer structures, Journal of Applied Physics 69 (1991) 2169–75.

[43] C. H. Henager, R. G. Hoagland, A rebound mechanism for misfit dislocation creation in metallic nanolayers, Scripta Materialia 50 (2004) 701–5.

[44] Y. Zhu, J. Narayan, J. Hirth, S. Mahajan, X. Wu, X. Liao, Formation of single and multiple deformation twins in nanocrystalline fcc metals, Acta Materialia 57 (2009) 3763–70.